The effect of Si/Al ratio on local and nanoscale water diffusion in H-ZSM-5: A quasielastic neutron scattering and molecular dynamics simulation study

Microporous and Mesoporous Materials 348 (2023) 112391

Contents lists available at ScienceDirect

Microporous and Mesoporous Materials

journal homepage: www.elsevier.com/locate/micromeso

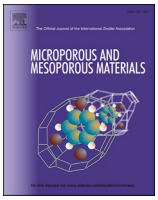

The effect of Si/Al ratio on local and nanoscale water diffusion in H-ZSM-5: A quasielastic neutron scattering and molecular dynamics simulation study

A.J. Porter [a], S.L. McHugh [a], T. Omojola [b], I.P. Silverwood [c,d], A.J. O'Malley [a,*]

[a] Centre for Sustainable and Circular Technologies, Department of Chemistry, University of Bath, BA2 7AY, UK
[b] Division of Fluid Dynamics. Department of Mechanics and Maritime Sciences. Chalmers University of Technology, 412 96, Göteborg, Sweden
[c] UK Catalysis Hub, Research Complex at Harwell, Science and Technology Facilities Council, Rutherford Appleton Laboratory, Oxford, OX11 0FA, UK
[d] ISIS Pulsed Neutron and Muon Facility, Science and Technology Facilities Council, Rutherford Appleton Laboratory, Didcot, OX11 0QX, UK

A B S T R A C T

The dynamics of water confined in H-ZSM-5 (protonated form of the Zeolite Socony Mobil – 5) has been studied using quasielastic neutron scattering (QENS) and classical molecular dynamics simulations (MD). QENS measurements probed water confined in ZSM-5 samples with Si/Al ratios of 15, 40 and 140 at 2.8 wt% loadings. In the lower silica samples, fitting of the elastic incoherent structure factor (EISF) showed that water diffusion was confined to a sphere (with radii ranging from 3.4 to 4.3 Å), suggesting the mobile water was located within the MFI (framework type of H-ZSM-5) channel intersections, giving localised diffusion coefficients in the range of ~0.9–1.8 $\times 10^{-9}$ m^2s^{-1}. In the high silica zeolite, the diffusion was observed to be far less confined and more long range in nature, with diffusion coefficients significantly higher than in the lower silica systems (~1.8–4.8 $\times 10^{-9}$ m^2s^{-1}). MD simulations further investigated the effect of the Si/Al ratio on water diffusivity at 2.8 wt% loading (9 molecules/unit cell (UC)) in H-ZSM-5 with Si/Al ratio = 15, 47, 95 and fully siliceous. The Si/Al ratio had a significant effect on the MD calculated nanoscale diffusivity of water, reducing the self-diffusion coefficient by a factor of 2 from a fully siliceous system to that with Si/Al = 15, due to the strong coordination and increased residence time of water molecules at the Brønsted acid sites which range from ~5 ps to ~2 ps in the Si/Al = 15 and Si/Al = 95 systems respectively. QENS observables, both the EISF and quasielastic line broadenings, were reproduced from the MD trajectories upon sampling the experimental timescale giving both qualitative and quantitative agreement with the QENS experiments. Fitting of the MD calculated EISF showed that the experimentally observed diffusion confined to a sphere of radii ranging from 3.5 to 6.8 Å was also present in our simulations, with diffusion coefficients calculated to within a factor of 0.5 of experiment.

1. Introduction

The confinement, and subsequent alteration in behaviour, of small molecules in zeolites is hugely important to a variety of applications [1], such as water decontamination [2], water softening – the largest use of zeolites by weight [3] – and catalysis, where water is an important side product. The rate at which water diffuses through a zeolitic system can have a significant effect on either the catalytic properties [4] or adsorption/separation properties [5] of the material. As such, the effect of zeolite composition, in particular the Si/Al ratio, on the behaviour of water is of great importance these applications.

Each aluminium substitution, and thus alteration in the Si/Al ratio requires the presence of a charge compensating cation (such as Na^+, Ca^+ or H^+). In particular, protons – which form Brønsted acid sites (BASs) – provide the catalytic sites utilised across zeolite catalysis [6]. Tuning the acidity of a microporous catalyst is important for such commercial applications [7] however multiple difficulties arise when choosing an appropriate Si/Al ratio in zeolite catalysts in particular. Although lower Si/Al ratios result in increased acid site density, and thus increased probability of an adsorbate meeting an active site, they also decrease the thermal stability of the zeolite and lower the acidity of each individual site [8]. This lowering in acidity takes place because more isolated BASs are more acidic due to a range of structural and electronic factors, in particular the electrostatic repulsion that would occur between two deprotonated acid sites in close proximity. This decreases the favourability of the deprotonated structure, increasing the deprotonation energy with the greater likelihood of proximal sites at lower Si/Al ratios [9]. Small molecules such as water or methanol, which demonstrate high diffusivity when unconfined, are significantly hindered by strong hydrogen bonding interactions with acid sites, as observed by a range of modelling [10,11] and spectroscopic studies [12–14].

Nanoscale water behaviour has been probed in a range of zeolitic systems via experimental techniques such as gravimetric studies, pulsed field gradient NMR (PFG-NMR) and quasielastic neutron scattering (QENS) as well as theoretical techniques such as molecular dynamics (MD) and Monte Carlo (MC) simlations [15–20]. The effect of Si/Al ratio

* Corresponding author.
E-mail address: a.o'malley@bath.ac.uk (A.J. O'Malley).

https://doi.org/10.1016/j.micromeso.2022.112391
Received 23 September 2022; Received in revised form 14 November 2022; Accepted 3 December 2022
Available online 5 December 2022

and the nature of the charge balancing counterion has been of particular interest across a range of studies. Parravano et al. [20] explored the effect of cation size, utilizing sodium and calcium forms of zeolite X and Y. In this early study, they observed, via PFG-NMR, insignificant differences in water mobility between NaX, CaX and CaY. Contrasting this, Paoli et al. [17] found that increasing the proportion of calcium – and thus the number of larger cations, in a zeolite A sample containing both sodium and calcium – decreased the water diffusivity. Our previous work [19] on water diffusion in faujasite (FAU) type zeolites employed molecular dynamics, finding a clear correlation between the Si/Al ratio and water mobility – with increasing numbers of BAS resulting in lower self-diffusion coefficients (particularly pronounced in the least siliceous zeolites). Both Humplik et al. [15] and Ari et al. [16] investigated the effect of Si/Al on water diffusion in MFI type zeolites, the framework family of ZSM-5, with the former employing water infiltration experiments and the latter computational methods. Humplik et al. reported that as the composition was varied from a fully siliceous sample to Si/Al = 100 the diffusivity was lowered by up to 2 orders of magnitude whilst Ari et al. used samples with Si/Al ratios of Si/Al = fully siliceous, 191 and 95 – where sodium was the charge compensating cation. Diffusion coefficients were reduced by a factor of ~5 at 297 K at the lowest Si/Al ratio of 95 compared to the fully siliceous zeolite. The effect of cation size also plays a large role in water behaviour in zeolites.

Nanoscale water behaviour in Brønsted acidic ZSM-5 is particularly relevant to catalytic conversions such as methanol-to-hydrocarbons related processes. The initial steps of methanol-to-olefin conversion involve an equilibration process of methanol, dimethyl ether (DME), and water with surface methoxy species and other adsorbed intermediates [21,22], where DME is a key adsorbed species due to its higher desorption energy than methanol [23], and decreasing the Si/Al ratio reduces the activation energies of desorption for both species in ZSM-5. Notably, DME desorption is not limited by its diffusion in ZSM-5 catalysts, and water reduces the reaction rates and leads to lower deactivation rates in methanol-to-olefins (MTO) compared to dimethyl ether-to-olefins (DTO) catalysis [24]. Understanding the influence of water on key descriptors such as desorption energies of DME is key to mechanistic insights into factors governing reaction rates. Moreover, the mobility of water molecules and the clustering effect of water on active sites have been shown to influence active site dynamics which could have a direct consequence for reaction rates [25,26].

From the broad range of works, it is clear that decreasing the Si/Al ratio, and thus including more cations, reduces the diffusivity of an adsorbate. It would follow that the same would be true for Brønsted acid sites although these are significantly smaller than any other charge compensating cation and thus could be expected to play a less significant role. Olson, Haag and Boghard [27] investigated the adsorption of water in H-ZSM-5, similar to the current study, via thermogravimetric analysis and found that the quantity of water adsorbed is proportional to the framework aluminium content. It may be expected that this increased adsorption may lead to reduced molecular diffusion. The adsorption of water to BASs in H-ZSM-5 has been probed in great detail using DFT, finding adsorption energies of −76 kJ mol^{-1} [28]. As well as classical forcefields giving adsorption energies of −64.4 kJ mol^{-1} [29], which also achieved excellent agreement with diffusivities measured by PFG-NMR [30]. In both cases the energy was evaluated using a single water molecule onto a BAS. To our knowledge, only our previous work [19] has studied the influence of systematic variation of Brønsted acid site concentration on water diffusivity, in any zeolite topology.

In terms of a combined experimental and theoretical approach to studying adsorbate behaviour in zeolite materials, combining QENS with molecular dynamics simulations has shown to be a uniquely powerful approach [31–33] due to their both probing timescales of 2 ps–100 ns depending on the instrument used. Neutron spectroscopy techniques are well suited to the study of (hydrogenous) molecular behaviour in porous inorganic materials due to their unique sensitivity to ^{1}H hydrogen [34] – and a system where the hydrogen content of the sorbent material is much lower than the adsorbed molecule population (such as water in Brønsted acidic zeolites) is particularly suited. As mentioned, MFI type zeolites are one of the most widely applied in both catalysis and adsorption processes. Although, studies probing diffusion in MFI zeolites with Brønsted acid sites are numerous, very few focus on the behaviour of water as an adsorbate, with no QENS studies of water in H-ZSM-5. In the current study, we probe the effect of the systematic variation in the number of Brønsted sites (Si/Al ratio) on water diffusivity in zeolite H-ZSM-5.

2. Experimental and simulation details

2.1. Quasielastic neutron scattering experiments

The QENS experiments employed 3 different H-ZSM-5 samples with Si/Al ratios of 15, 40 and 140. The samples are sourced from Zeolyst International (CBV3024E, CBV8014 and CBV28014 respectively). Each sample was obtained in its ammonium form and subsequently converted to its H-ZSM-5 form by heating from room temperature to 798 K for 4 h in atmosphere, at a heating rate of 5 K min^{-1}. The final chemical formula for each experimental H-ZSM-5 sample is $H_nAl_nSi_{96-n}O_{192}$ where n = 0.68, 2.3 and 6 at Si/Al = 140, 40 and 15 respectively. The samples were then dried for 4 h, ramping up the temperature at 1 K min^{-1} to 393 K under vacuum to avoid the dealumination of the framework before loading. To load the samples, the dry samples were weighed and left in atmosphere until the desired loading was reached (2.8 wt%) or 9 molecules per unit cell (mol/UC). This water loading is below the maximum water uptake for silicalite-1 (pure silica ZSM-5) at equilibrium, shown to be 3 wt% in previous adsorption studies [35]. The empty (dry) and loaded samples were then transferred to thin-walled aluminium cans of annular geometry where a 1 mm annulus was used to avoid multiple scattering from the sample; this was all carried out in an inert atmosphere in the case of the dry sample. The QENS experiments were carried out using the OSIRIS spectrometer [36] at the ISIS Pulsed Neutron and Muon Source. The aluminium cans were placed in a top-loading closed-cycle refrigerator. Initially, the samples were cooled to a base temperature of approximately 6 K for a resolution measurement and subsequently heated to 300, 330 and 360 K for QENS measurements. This gave a range of temperatures but remained below the vaporisation temperature of water, avoiding pressurisation of the sample container as a safety precaution. Using TGA (as detailed and discussed section SI 3.1) we have confirmed for the Si/Al = 14 and 40 samples that the 2.8 wt% content of water loaded at ambient conditions would also be present and stable in the systems at the highest measured temperature of 360 K. However in the Si/Al = 140 system at 360 K we have not been able to confirm this. We suggest that any comparison between the water content observed from an open sample undergoing TGA with that in a sealed can at equilibriium would not be exact. However, we also suggest that any direct comparisons of diffusivity between the MD simulations in the Si/Al = 140 system at 360 K (using the same loading as ambient temperature), and those of the QENS studies at this temperature should be treated with caution, as these may have a lower loading due to desorption. The 002 reflection from the pyrolytic graphite analyser was used, giving an energy resolution of 24.5 μeV at FWHM with energy transfers measured in a window of ±0.55 meV. The detectors cover measurements over a Q range of 0.2–1.8 $Å^{-1}$. The neutron scattering signal from the empty zeolite samples was also measured (which contain a very low quantity of hydrogen) and the signal was subtracted from the water loaded samples – leaving only the signal relating to the water itself. This also removes any minor scattering from the Al sample vessel. All QENS data were fitted and processed using the neutron scattering analysis packages DAVE [37] and Mantid [38].

2.2. Molecular dynamics simulations

The setup and running of the molecular dynamics simulations shall

now be detailed.

2.2.1. MFI framework

The siliceous MFI orthorhombic unit cell [39] (UC) of 288 atoms with Pnma symmetry (with dimensions of (a = 20.0900 Å, b = 19.7380 Å, c = 13.1420 Å) was systematically substituted with aluminium to reach the Si/Al ratios of; fully-siliceous (0 Al per UC), 95 (1 Al per UC), 47 (2 AL per UC), and 15 (6 Al per UC). The aluminium atoms were placed into their most thermodynamically stable positions – the T14 site (equivalent to the T2 site in the Orthorhombic cell) [40,41] as far apart as possible from their nearest neighbour to abide by Dempsey's rule [42] while accounting for the later implementation of periodic boundary conditions. The unit cell of the Si/Al = 15 structure is shown in figure SI 1 where the Al substitution and proton positions are depicted. The protons of the Brønsted acid sites (denoted O_b-H_b) are shown in Fig. 1A (where silicon is shown in yellow, oxygen in red and hydrogen in white) and are accessible via the sinusoidal channels, or within an intersection of the two channels. The unit cells were then extended to create 2 × 2 × 4 (40.2 Å × 39.5 Å × 52.6 Å) supercells of ca. 4600–4700 framework atoms – depending on Si/Al ratio - and periodic boundary conditions were employed – Fig. 1. While the framework was treated as flexible, the total volume of the supercell was kept at these dimensions regardless of Si/Al ratio. All snapshots of the simulation were generated using Aten 2.1.9 [43].

The same potential model was used as in our previous work investigating water diffusion in H-FAU [19] which employed the potentials of Schröder et al. [44] – derived from empirical fitting to structural and physical properties of α-quartz, by Sanders et al. [45], and Al_2O_3, by Catlow et al. [46], to describe a flexible zeolite framework. The assigned framework atomic charges are shown in Table SI 2.1.1. To maintain the structural stability in low silica zeolites, the three-body potential – for mediating O-T-O angles – was replaced by those employed by Ramsahye and Bell [47]. This three-body potential is based on that derived by Kramer et al. [48] using ab initio methods and fitting to the vibrational spectrum of α-quartz, modified by scaling and further fitting to crystal structure data of low silica zeolites. A full list of the parameters used to model the framework is compiled in Table SI 2.1.2. Before water loading, the framework was equilibrated to 300, 330 and 360 K via MD simulation using DLPOLY 4 code [49] in the NVT ensemble using a Berendsen [50] thermostat, and a timestep of 0.5 fs until thermal and energy fluctuations had stabilised, requiring at least 80 ps.

2.2.2. Water loading

Following the construction and equilibration of the empty framework supercells, water molecules were added as shown in Fig. 2. 144 molecules per supercell were added to achieve a loading of ~2.8 wt% (9 molecules per unit cell). The water molecules were described by a flexible TIP3P model derived by Schmitt and Voth [51], assigning the water oxygen (O_w) and hydrogen (H_w) charges of −0.834 and +0.417 respectively – the parameters of which are listed in Table SI 2.1.3. The intramolecular bond stretching and bending parameters were derived to reproduce geometrical and energetic quantities of selected $H_3O^+ \bullet nH_2O$ clusters and refinement using quantum mechanical calculations. For the water-zeolite interactions, two sets of potentials have been used. Firstly, the potentials of Du and de Leeuw [52] which were obtained from DFT calculations of water adsorption on α-quartz, are used to describe the interaction of water with the Brønsted sites and oxygen of the framework. Additionally, the potentials of Lewis et al. [53] were used to describe the Si^{4+} and Al^{3+} interaction with water. These are an updated version of those from Du and de Leeuw by increasing the repulsive term to avoid very close contact of the water with these species which results in unfeasible structures. The full list of potentials is shown in Table SI 2.1.3.

The water-containing cells were energy minimised to stabilise the initial configuration of water molecules loaded into the zeolite framework before the system was equilibrated.

2.2.3. Molecular dynamics procedure

$$D_s = \frac{1}{6}\lim_{t\to\infty}\frac{d}{dt}\left[\{r(t) - r(0)\}^2\right] \quad (1)$$

All MD trajectories were generated using the DLPOLY 4 code [49] with a timestep of 0.5 fs, using a van der Waals cutoff of 10 Å and the Coulombic interactions were treated using the Ewald method. The Berendsen [50] thermostat was used to control the temperature in the canonical ensemble, during the equilibration run over 100 ps, with simulations run at 300, 330 and 360 K. The simulations were then run for a total of 2 ns in the microcanonical ensemble with the atomic positions recorded every 0.1 ps. The self-diffusion coefficient (D_s) was calculated using the Einstein relation, shown in equation (1).

This involved tracking the positions of the oxygen atom of each water molecule and calculating the mean squared displacement (MSD) across all molecules for each step of the simulation. The use of the Einstein relation was verified by confirming the log(MSD)-log(t) relationship was linear.

The method of multiple time origins was used to improve the statistics of each simulation. An MSD plot over the first 1 ns was taken, with further MSDs taken starting at an offset of 1 ps from the origin (i.e. 0-1000 ps, 1–1001 ps, 2–1002 ps, etc.) until the whole 2 ns simulation was covered. The average of the resulting 1000 × 1 ns MSD plots was

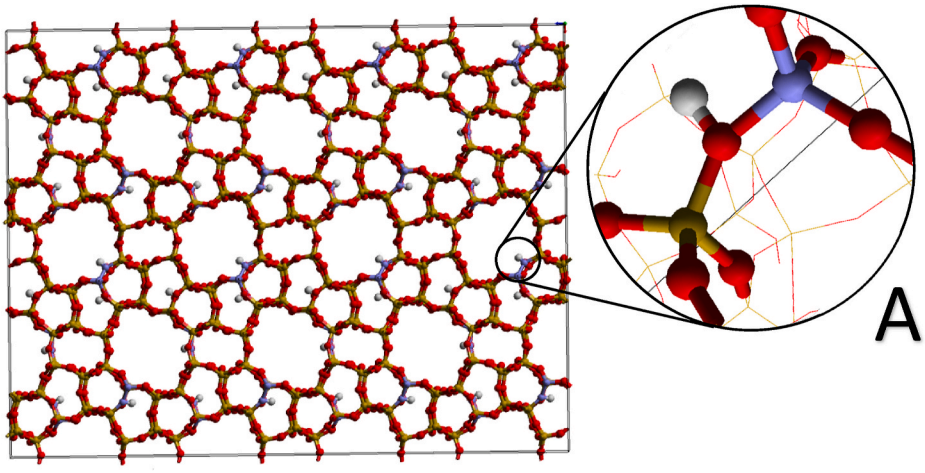

Fig. 1. The Si/Al = 15 MFI supercell used in our MD simulations, viewed from the 010 direction. Silicon (yellow), oxygen (red) and aluminium (blue). '**A**' shows a magnified snapshot of a Brønsted site. (For interpretation of the references to colour in this figure legend, the reader is referred to the Web version of this article.)

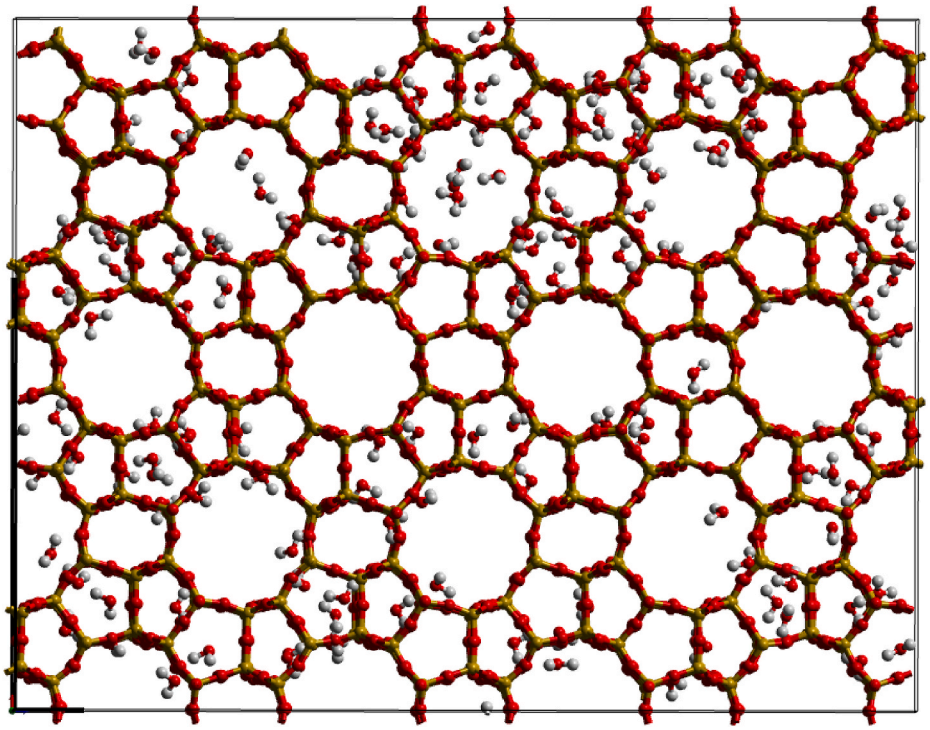

Fig. 2. Snapshot of a siliceous MFI framework supercell loaded with water to 2.8 wt% viewed from 010 direction.

then taken from which the diffusion coefficient was then calculated. The diffusion coefficient was calculated from the linear portion of the MSD plot, adhering to the Einstein relation. To remain consistent across all systems, this was taken from 200 ps to 1 ns of the MSD as all systems remained linear in this portion. The error was evaluated by calculating the variance of five diffusion coefficients, each calculated over fractions of the MSD used to calculate the diffusion coefficient.

To probe both the differing sorbate-sorbate interactions and sorbate zeolite interactions in each MD run, radial distribution functions (RDFs) were calculated using the atom trajectories from the MD simulations. This was carried out using the integrated module for RDFs within the Visual Molecular Dynamics [54] package.

To probe the interactions between the water molecules and the Brønsted acid sites, specifically in terms of residence times, the contact correlation function between O_w and H_b was also calculated, using the method described in section SI 2.0.

QENS observables were also produced from the simulations by calculation of the intermediate scattering function (ISF), allowing for direct comparison with our experiments. The atomic positions were used to calculate the intermediate scattering function (shown as the powder average expression):

$$F_s(Q,t) = \frac{1}{N}\sum_{i=1}^{N}\left\langle \frac{\sin(Q|d_i(t+t_0) - d_i(t_0)|)}{Q|d_i(t+t_0) - d_i(t_0)|}\right\rangle \quad (2)$$

where N is the total number of atoms and d_i is the vector from the molecule's centre of mass to one of the hydrogen atoms at time t. The ISF is directly measured in the QENS experiments and thus its calculation allows for direct comparison across experiment and simulation. The method of multiple time origins was also used in the calculation of the ISF, where thirty 64 ps trajectories were generated, spread equally over the entire 1 ns simulation. A 64 ps sample length was chosen as this relates to 0.025 meV – the width of the resolution function of the OSIRIS spectrometer. The resulting ISF may then be fit with an exponential function of the form:

$$F_s(Q,t) = B(Q) + \sum_{n=0}^{i} C_n e^{-\Gamma_n t} \quad (3)$$

Where i is the number of exponentials required for satisfactory fitting and $B(Q) + \sum_{n=0}^{i} C_n = 1$. The baseline values – $B(Q)$ – correspond to the elastic incoherent structure factor (EISF) as it relates to the atomic arrangement at $t \to \infty$, thus providing the molecular rotation symmetry. Therefore, the baseline can be plotted as a function of Q in an analogous procedure to the QENS experiments and Γ_i is equivalent to the half-width half-maximum (HWHM) of the quasielastic scattering function (or dynamical structure factor) and as such may be used to calculate the rates of translational motions over the probed timescales.

2.3. Sample characterisation

All three ZSM-5 samples underwent characterisation via XRD and TGA as previously mentioned. These are described in detail in the supplementary information (SI3). The major crystalline phases of both samples were confirmed to be MFI as detailed.

3. Results and discussion

3.1. Quasielastic neutron scattering experiments

QENS spectra for water in H-ZSM-5 samples of the different Si/Al ratios at 300 K are shown in Fig. 3. Each of the QENS spectra were fit to a delta function convoluted with the resolution measurement taken at 6 K, a Lorentzian function to capture the quasielastic broadening and a flat background to account for motions taking place outside the experimental window and the Debye-Waller factor. These are shown in Fig. 3 – examples of individual plots and their fits are shown in SI1.3.

All three samples show measurable dynamics, illustrated by the discernible Lorentzian function which appears to increase in size as the Si/Al ratio is increased. Notably, the decay of the elastic peak with Q is more significant as the Si/Al ratio is increased – suggesting a higher level of mobility is present in the most siliceous sample. The relative contri-

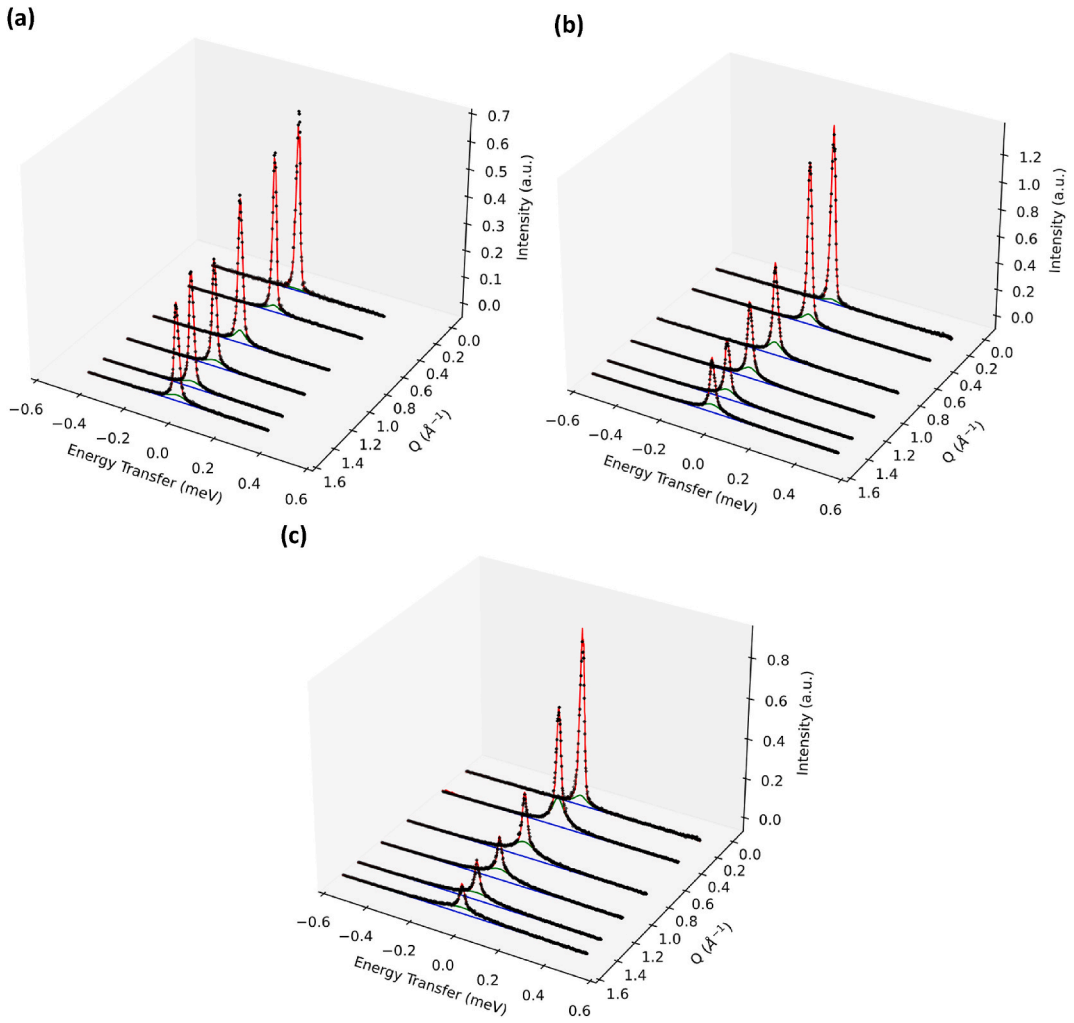

Fig. 3. Subtracted QENS spectra of water in H-ZSM-5 with (a) Si/Al = 15, (b) Si/Al = 40 and (c) Si/Al = 140 at 300 K at Q = 0.22, 0.48, 0.86, 1.14, 1.39 and 1.54 Å^{-1}. Selected spectra shown for clarity. Experimental values are shown as black dots, red lines for total fit, blue line for background and green line for the Lorentzian component fit to the broadenings. (For interpretation of the references to colour in this figure legend, the reader is referred to the Web version of this article.)

butions of the elastic and quasielastic scattering, illustrated by the Lorentzian function, is quantified using the elastic incoherent structure factor (EISF) which gives insight into the geometry of motions occurring – equation (4).

$$A_0(Q) = \frac{I_{elastic}(Q)}{I_{elastic}(Q) + I_{inelastic}(Q)} \tag{4}$$

This is calculated by taking the area of the delta function and dividing it by the total area of the scattering function. Initial fitting to the Si/Al = 15 system is shown in figure SI 1.3.1.

A series of models may be applied to fit the EISF, each of which gives information about the nature of water behaviour such as isotropic rotation which describes a molecule whose protons are rotating randomly about its centre of mass (Fig. 4a), uniaxial rotation or jump diffusion around 2 equivalent sites on a circle (2-site rotation) where the molecule undergoes a rotor-like motion around its C_2 axis (Fig. 4b), or the model of diffusion confined to a sphere of a given radius derived by Volino and Dianoux (the VD confined diffusion model), whereby the molecules are confined and translate within a sphere of a given radius (Fig. 4c). Schematics of these motions are shown in Fig. 4.

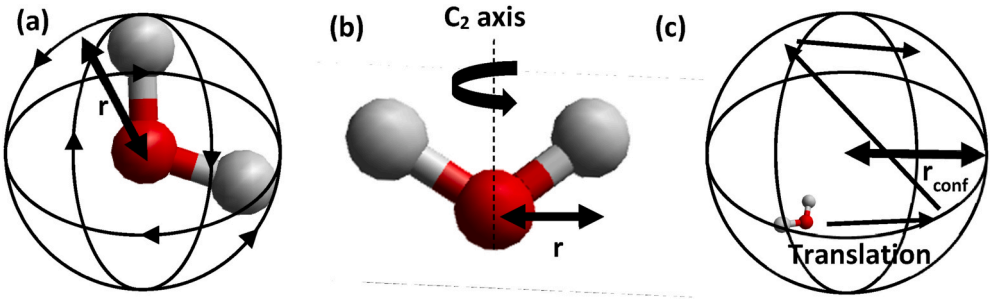

Fig. 4. Examples of characteristic motions used to model the elastic incoherent structure factor where (a) is an isotropic rotation, (b) a two site or uniaxial rotation and (c) diffusion confined to a sphere.

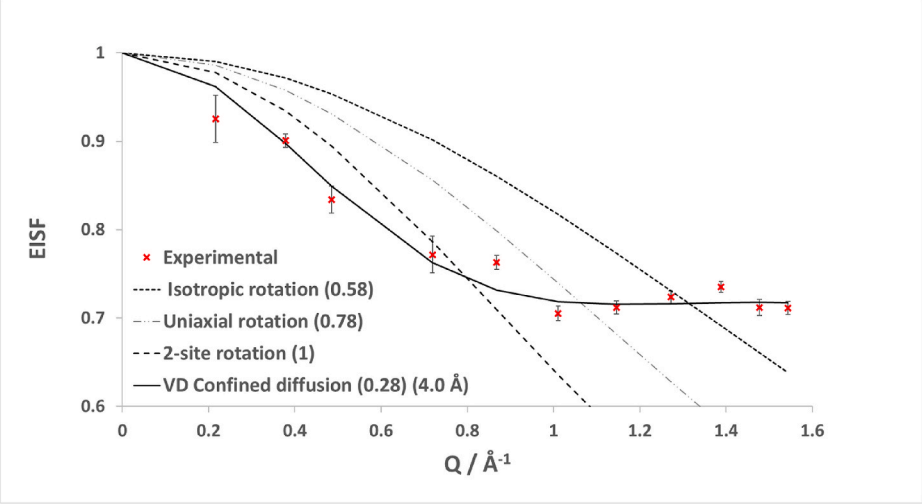

Fig. 5. Experimental EISF plot for water in H-ZSM-5 with a Si/Al = 15 at 300 K. Models for confined volume and isotropic, 2-site and uniaxial rotation – mobile fractions and relevant radii are included in brackets.

As shown in figure SI 1.3.1, none of the models used in their pure form can fit the experimental points, and thus the incorporation of a mobile fraction, which accounts for a population of water molecules being immobile on the timescales observed by the instrument was necessary. Full details of the models and the scaling of the EISF to incorporate the mobile fraction may be found in the supplementary information SI 1.1. The scaled models and their best fits to the data (Si/Al = 15, 300 K) are shown in Fig. 5.

The fits from each Si/Al ratio at 300 K are also shown in Fig. 6 with the fits for 330 and 360 K found in SI1.3. A clear decrease in the EISF and thus an increase in total mobility of water in the system is observed as the systems become more siliceous.

When scaled, the Volino–Dianoux (VD) model of diffusion confined to a sphere gave the best fit to the data, necessitating a mobile fraction of 28.5% and a confining radius of 4 Å at 300 K for the Si/Al = 15 sample – both of which have been allowed to vary in the data fitting. The mobile fractions and confined radii extracted from the fits for each system and temperature are shown in Table 1.

The radius of the sphere to which diffusion is confined is significantly larger in the more siliceous systems than those of the Si/Al = 15 and 40 systems (~4 Å in the lower Si/Al systems compared to ~7 Å in the more siliceous system). The typical radius of an MFI pore is approximately 2.75 Å, significantly smaller than the radii observed here. The radius of a ZSM-5 channel intersection, however, ranges from ~3.5 to 4.5 Å – depending on whether BASs are present or not [14]. Both the Si/Al = 15 and 40 systems fall within this range, suggesting that the water which is mobile on the instrumental timescale is diffusing within the channel intersection. The large radius observed in the Si/Al = 140 system suggests that the diffusion is significantly less confined and takes place over a longer length-scale. Indeed, the significant quasielastic signal at low Q suggests a significant proportion of the molecules are undergoing free

Table 1
Parameters of the Volino-Dianoux diffusion confined to a sphere model giving the best fit to experimental EISF values. Radii are quoted to the closest 0.5 Å

		Si/Al ratio		
Temperature (K)		15	40	140
300	Mobile fraction	0.284	0.489	0.758
	Radius (Å)	4.0	4.0	5.0
330	Mobile fraction	0.349	0.592	0.763
	Radius (Å)	4.0	4.0	6.5
360	Mobile fraction	0.390	0.628	0.792
	Radius (Å)	4.0	4.0	7.0

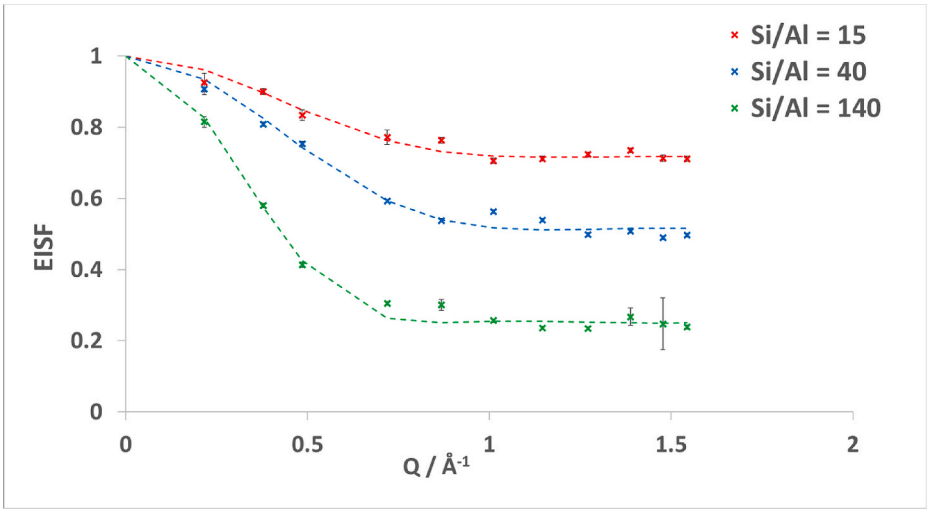

Fig. 6. Experimental EISF plots and the fit of a model of diffusion confined to a sphere for water in the Si/Al = 15, 40 and 140 H-ZSM-5 samples at 300 K.

diffusion with minimal confinement. It is therefore clear that this model of diffusion confined to a sphere is not adequate to fully describe all the motions, however we employ it for direct comparison with the dynamics observed in the other sample. Ultimately, the specifics of the fit to the QENS data – in this case – may not be entirely representative of the motions the water is undergoing. We may well be seeing a combination of both confined motions and free diffusion which are not possible to deconvolute given the nature of the dataset.

Upon concluding the presence of translational water diffusion confined to a sphere matching the radius of a ZSM-5 intersection (though significantly less confined for the most siliceous zeolite sample) from the EISF analysis, the diffusivity may be quantified using the half-width at half-maxima (HWHM) of the Lorentzian functions fit to the scattering functions, and their Q^2 dependence – determining the rates of motion. The fitting of the EISF to the Volino-Dianoux model of diffusion confined to a sphere suggests that the Q^2-dependence of the HWHM would be expected to conform to a model of translational diffusion. These include Fickian diffusion (a DQ^2 dependence) or jump diffusion (a deviation from the Q^2 dependence at higher Q values per the Chudley-Elliot [55] or the Singwi-Sjölander [56] jump diffusion model), however, below a Q value commensurate with a length matching the radius of the confining sphere($Q = \pi/r_{conf}$), a plateauing/Q-independence of the HWHM will be observed, deviating from the model as previously shown for ammonia diffusion in Levynite [55].

Due to the confinement of the molecules, the plateauing of the Q-dependence indicative of the VD model confined diffusion model is observed at low Q – demonstrating that the molecules are not mobile over these longer ranges on the timescale probed by our spectrometer. At the higher Q values, the data from all three systems were best fit to the Singwi-Sjölander [56](SS) jump diffusion model – described in full in SI1.2. The best fit to the QENS data from the two lower Si/Al ratio systems had mean jump distances of approximately ~1 Å and residence times ranging from 7 to 9 ps. This fit slightly changes at each temperature as shown in Fig. 7.

The QENS broadenings of water in H-ZSM-5 (Si/Al = 140) and their fits, as shown in Fig. 7b, are significantly larger than those in the systems with more acidic sites, illustrating a significant increase in diffusivity. We also note that a plateauing is not completely clear at the lower Q values in Fig. 7b, though an exact fit to the unconfined jump model cannot be confirmed either. The need to employ the Volino-Dianoux model with a confining radius of ~7 Å to our EISF in Fig. 6 suggests that a level of confinement and restriction is clearly present, but that the model of complete confinement to a sphere observed at the lower Si/Al ratios, while necessary given the fitting of the EISF, is less exact this case. The parameters of each fit for all three systems at each temperature are also shown in Table SI 1.3.1.

Similar trends are observed in both the Si/Al = 15 and Si/Al = 40 systems, both with comparable residence times (~9.2–7.2 ps) and similar jump distances of ~1 Å. The Si/Al = 140 system gives residence times almost half those of the Si/Al = 14 and 40 samples, but similar jump distances, suggesting that water is significantly more mobile in this system. Across all three systems the diffusion coefficients, calculated from the SS jump model (as opposed to those using the Volino confined diffusion model – which would take into account the confining radius), range from ~1 to 5×10^{-9} m^2s^{-1} as shown in Table 2. These diffusion coefficients fall in a similar range to that of DME at a loading of 12 wt% in H-ZSM-5 (Si/Al = 35) [14]. The full list of diffusion coefficients may be found in section SI 2.3. Water across all systems, although confined, is

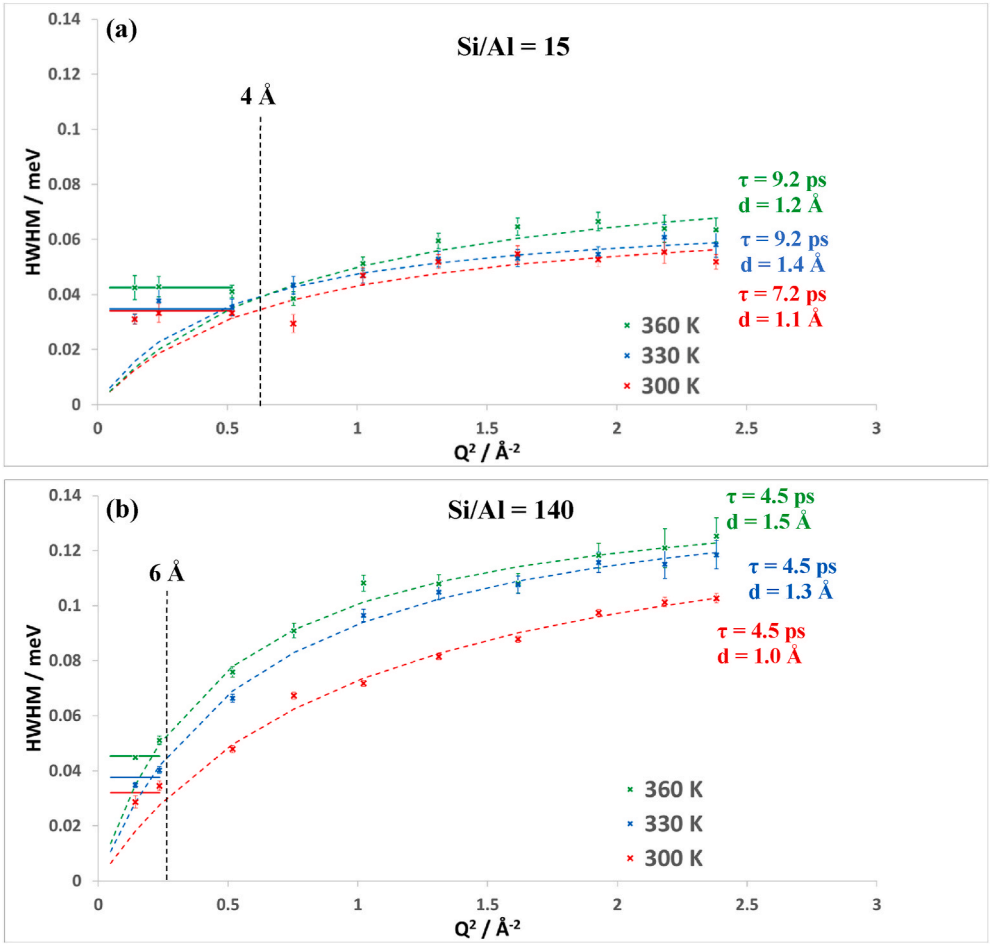

Fig. 7. Experimental HWHM plots for water in the Si/Al = 15 and 140 ZSM-5 at 300, 330 and 360 K as well as the lines of best fit.

Table 2
Self-diffusion coefficients (1×10^{-9} m^2s^{-1}) obtained from the QENS experiments calculated from the FWHM fitting of the Singwi-Sjolander jump diffusion model in the Si/Al = 15, 40 and 140 MFI at 300, 330 and 360 K.

Self-diffusion coefficient (10^{-9} m^2s^{-1})			
	Si/Al ratio		
Temperature (K)	15	40	140
300	1.61	1.19	2.19
330	2.16	1.51	3.70
360	1.67	1.73	4.90

still moving with diffusivity similar to that of unconfined water which has a D_s of 2.3×10^{-9} m^2 s^{-1} at 298.15 K as measured by PFG-NMR [57].

According to the Volino-Dianoux model of diffusion confined to a sphere, the confined diffusion coefficient is related to the HWHM of the scattering function by $HWHM = 4.33\frac{D}{r_{conf}^2}$, and this diffusion coefficient is considered more reliable than that obtained using the jump diffusion model as the broadenings used are those at lower Q values, probing motion over longer distances. These are listed in Table SI1.3.2 and plotted in Fig. 8.

In the Si/Al = 15 and Si/Al = 40 systems, similar confined diffusion coefficients are observed ranging from 0.8 to 1.8 $\times$ 10^{-9} m^2s^{-1} across both zeolites – in the same range as that calculated using the SS jump model. The Si/Al = 140 system shows a much wider range from 2.6 to 4.8 $\times$ 10^{-9} m^2s^{-1}, with increased water diffusivity by up to a factor of ~3 compared to its less siliceous counterparts at each temperature, suggesting that the motions in this system are no longer localised and that water in this system is far less confined and hindered.

Activation energies can then be calculated from these diffusion coefficients resulting in E_a values of 6.1 $\pm$ 3.5, 10.8 $\pm$ 10 and 13.3 $\pm$ 1.5 kJ mol^{-1} in the Si/Al = 15, 40 and 140 systems respectively, illustrating the larger increase in diffusivity with temperature with a lower concentration of BASs. These are significantly higher than those observed by Omojola et al. [14] for methanol (0.58 kJ mol^{-1} in HZSM-5(135) at 14 wt% loading) and DME (0.96 and 1.33 kJ mol^{-1} in HZSM-5(36 and 135) respectively at 12 and 10 wt% loading). The authors express caution in any trends inferred from the referenced study, due to large errors obtained, however, the clear difference in activation energy between water and these two species indicates the strength of water interactions within the zeolite. The loading differences between the two samples may also be a contributing factor. A general increase in the activation energy of diffusion is observed as the Si/Al ratio is increased which seems counterintuitive given the larger diffusion coefficients at lower aluminium content. The activation energy, however, does not take into account the mobile fractions which decrease with the aluminium content. As discussed in the following section, this does not align with the results obtained from the classical simulation and as such another approach may be necessary. The formation of hydronium ions, shown recently in the literature [58,59] – due to their relevance to catalytic activity [60], may also play a role in the measured activation energies which could not be accounted for in the following classical simulations.

The trends in diffusivity are of particular interest in the context of methanol to hydrocarbons catalysis when compared with the other relevant species studied by QENS. In the Si/Al = 40 system, higher self-diffusion coefficients for water are obtained by a factor of ~1.5 and ~1.75 than DME and methanol respectively in ZSM-5 (Si/Al = 36) [14]. As mentioned in the introduction, DME, has a higher activation energy of desorption than methanol (121 vs 112 kJ mol^{-1} over ZSM-5 (Si/Al = 25)). Calculation of the desorption energy for water in ZSM-5 (Si/Al = 15) takes place between 40 and 60 kJ mol^{-1} leading to its favourable displacement by methanol [61,62]. This relatively weak desorption energy of water would lead to it moving relatively quickly in comparison to dimethyl ether and methanol in the ZSM-5 channels occupying freely available Brønsted acid sites. It may be expected that due to the faster diffusion of water, more sites will be initially covered by water molecules which will subsequently reduce the reaction rates during steady-state MTO conversion. This has also been observed in the literature whereby organic molecules appear to adsorb in partly filled pores which are not occupied by hydrated hydroxonium ion clusters [59].

4. Molecular dynamics simulations

In the following section, the results of the molecular dynamics simulations pertaining to the effect of the Si/Al ratio and temperature on the self-diffusivity of water in H-ZSM-5 are discussed. The mean squared

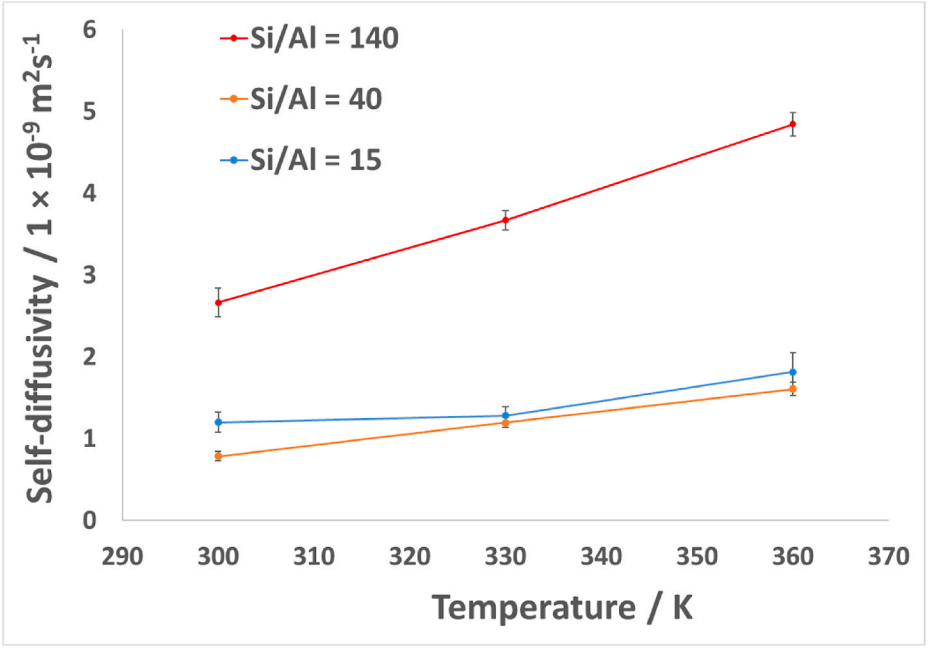

Fig. 8. Self-diffusion coefficients obtained from the QENS experiments calculated from the FWHM of the Volino-Dianoux model in the Si/Al = 15, 40 and 140 MFI at 300, 330 and 360 K.

displacement plots of the water confined with the Si/Al = 15, 40, 95 and siliceous MFI frameworks at 300 K are shown in Fig. 9.

All systems show reasonable linearity in their MSD plots from 200 ps onwards and thus the self-diffusion coefficients were calculated using the Einstein relation, equation (1), in this region and are listed in Table 3.

As the Si/Al ratio is decreased, and more BASs are introduced, the water diffusivity decreases from 1.31 to 0.65 $\times$ 10^{-10} m^2s^{-1} at 300 K and from 6.21 to 2.58 $\times$ 10^{-10} m^2s^{-1} at 360 K. As in previous work investigating water diffusion in zeolite Y [19] and methanol in H-ZSM-5 [10], a stronger dependence is observed at lower Si/Al ratios – illustrated in Fig. 10.

This behaviour is caused by strong interactions between the water molecules and BASs, shown in Fig. 11, as illustrated by the RDFs shown in Fig. 12 showing a range of possible hydrogen bonds.

Firstly, looking to Fig. 12a which shows the H-bond between water oxygen and BAS hydrogen, we can observe an intense peak at ~2.2 Å, which has a slight broadening suggesting that many molecules lie within this range of primary coordination. This geometry of coordination and strength has also been demonstrated in H-ZSM-5 by previous inelastic neutron scattering studies [63] which were performed in direct comparison with *ab initio* calculations [64]. Two additional peaks are seen at 3.5 and 4.75 Å with the former not appearing in the Si/Al = 15 system. The latter interaction may be attributed to a secondary coordination shell, given that it lies ~2.5 Å further away than the primary coordination shell – close to the equilibrium distance between two water molecules. The interaction at 3.5 Å in Fig. 12A is likely an alternative bonding mode between the water molecule and the BAS – these, however, are difficult to deconvolute from the trajectories as the water is very labile in these positions. Less proximate bonding modes will be decreasingly likely with reduced Si/Al ratio due to the higher frequency of BAS that the water may bond to, and hence the peak representing this interaction is not seen in the Si/Al = 15 system. Based on the vicinity of the primary coordination, it is clear that the predominant hydrogen bond is through the $H_b - O_w$ interaction. The $H_w - O_b$ interaction, shown in Fig. 12b, shows similar behaviour but is essentially a consequence of the $H_b - O_w$ interaction, with the initial peak appearing at ~3.5 Å. There are very limited interactions between the water and the non-BAS framework oxygens, Fig. 12c, with the water having an almost equal probability of lying at any distance above 2 Å from the framework, supporting the conclusion that the slowing of the water diffusion is due to the interaction with the BAS.

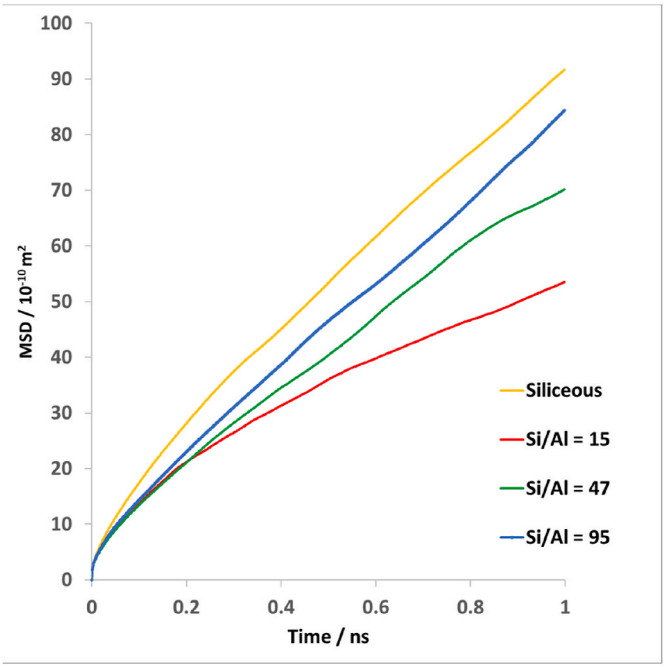

Fig. 9. MSD plots of water confined in the Si/Al = 15, 40, 95 and siliceous ZSM-5 systems from the MD simulations.

Table 3
MD calculated self-diffusion coefficients of water in H-ZSM-5 with Si/Al ratios of 15, 47, 95 and siliceous at 300, 330 and 360 K.

	Self-diffusion coefficients (10^{-10} m^2s^{-1})		
Si/Al ratio	300 K	330 K	360 K
15	$0.65_{\pm 0.17}$	$1.11_{\pm 0.33}$	$2.58_{\pm 0.32}$
47	$1.06_{\pm 0.35}$	$1.75_{\pm 0.19}$	$3.86_{\pm 0.03}$
95	$1.25_{\pm 0.05}$	$2.38_{\pm 0.18}$	$5.11_{\pm 0.71}$
Siliceous	$1.31_{\pm 0.06}$	$2.60_{\pm 0.09}$	$6.21_{\pm 0.16}$

The activation energy of water diffusion in H-ZSM-5 for each Si/Al was also calculated – shown in Table SI 2.2.1 ranging from 19 to 23 kJ mol^{-1}. No clear trend in activation energy is observed and insignificant differences are seen between the activation energies across all systems when the errors are taken into account, but they are consistently higher than those obtained experimentally. As well as the diffusion coefficients being lower, we note that the scale of mobility probed is significantly larger than those probed by our QENS experiments, modelling the nanoscale mobility throughout the whole supercell rather than the more localised motions discussed in the experimental section. Comparing to previous MD simulations of methanol in H-ZSM-5 [10], the activation energies here are significantly larger (by 10–15 kJ mol^{-1}), as one would expect given the larger orientational dependence of methanol hydrogen bonding, both with the zeolite and between methanol molecules. This orientational dependence would logically lead to a lower frequency of said H-bonding interactions, so their influence on the activation energy would be lower. The number of molecules per unit cell (MPUC) is also higher by 4–6 molecules in our water systems (loading of 9 MPUC) therefore we expect sorbate-sorbate interactions to play a more significant role in the water systems and consequently increase the activation energies.

The contact between water and the BAS can be further probed using the contact-correlation function which calculates the average residence time of a water molecule on the site using the same methodology described in previous work [19] – see section SI 2.0 for further details on the methodology. The residence times range from 4.7 ps in the Si/Al = 15 system to 2.1 ps in the Si/Al = 95 system, with a clear negative correlation shown between the Si/Al ratio and H_2O residence time – shown in figure SI 2.2.1. This is most likely due to the presence of more BASs in the system which reduces the chance of water being freed from the site by adsorbate-adsorbate interactions. These residence times are similar to those observed for water in FAU at 5 wt% loading around ~5 ps, [19], although a much higher dependency on Si/Al ratio is observed in MFI. This may be due to the reduced pore size in the MFI compared to FAU – increasing the likelihood of water-BAS contact – thus increasing this dependence. The adsorption energy of a single water molecule onto a BAS within the framework was also evaluated using an energy minimisation (using the conjugate gradients method within DLPOLY) of the relevant structures. The adsorption energy was calculated to be −72 kJ mol^{-1} – falling well within the range reported in other literature (detailed in the introduction).

The reduced water-water interactions, as the Si/Al ratio is decreased, are further evidenced by the RDF plots in Fig. 13 which shows the RDF between the oxygens of the water molecules.

The initial peak at ~2.75 Å shows the equilibrium distance between two water oxygens which shows a clear decline in the intensity of this initial peak as more BASs are introduced into the system. The integral under this peak relates to the number of water molecules within the given distance and thus shows that the water molecules are forming smaller clusters as the Si/Al ratio is decreased. This can be explained by there being more BASs to distribute the water molecules over and thus

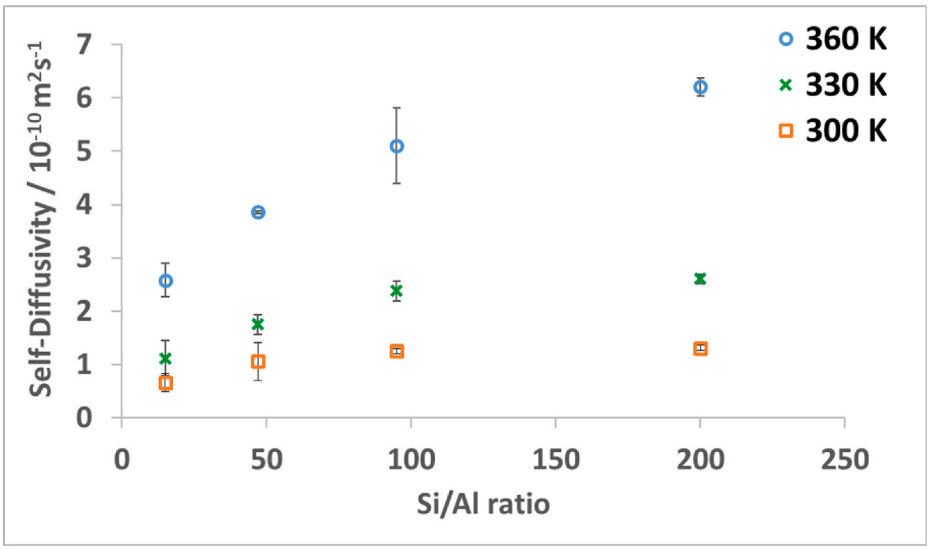

Fig. 10. Self-diffusion coefficients of water confined in the Si/Al = 15, 40, 95 and siliceous MFI frameworks at 300, 330 and 360 K using MD simulations.

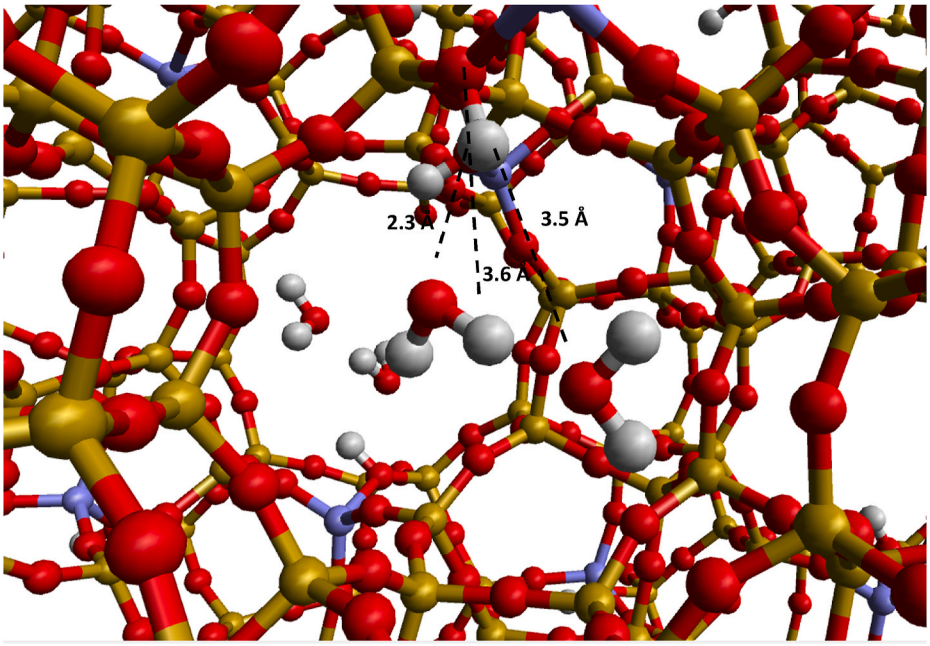

Fig. 11. Snapshots illustrating possible hydrogen bonds between water and the acid sites of the H-ZSM-5 framework.

the formation of larger water clusters is less likely in the lowest Si/Al ratio systems. This correlates with the observed decrease in diffusivity with Si/Al ratio as water which is not interacting with a BAS will exhibit higher mobility.

QENS observables were also reproduced via calculation of the intermediate scattering function. The calculated ISF is then fit using an exponential function as shown in figure SI 2.3.1. The parameters of this fit relate to QENS observables as described in sections SI1.1 and SI1.2. A satisfactory fit is achieved with two exponential functions.

The baseline of the exponential fit to the ISF at each Q value is then plotted as a function of *Q* to create an MD calculated EISF, an example of which is shown in Fig. 14. Upon fitting the MD calculated EISF to the same models used in the QENS experiments, it was found The Volino-Dianoux (VD) model of diffusion confined to a sphere shows by far the best fit of all the single models (when a mobile fraction of 0.86 is introduced). However, a better fit is achieved by a linear combination of the Volino-Dianoux confined diffusion model and the model of isotropic rotation (where a varying weighted contribution of these models to the overall fit is considered) and no immobile fraction is necessary.

This combination of models fits the EISFs calculated across all systems and temperatures. The parameters such as the radius of the confining spherical volume and the fractional contribution of the Volino-Dianoux model are shown in Table 4. This fit has two freely varying parameters; the confining radius and the weighting of the confined diffusion model in the fit against that of the isotropic rotational model. Both the isotropic rotation radius and mobile fraction (100%) were kept fixed.

The proportion of confined translational motion increases with temperature, similar to the mobile fractions observed by QENS. The fraction of molecules undergoing confined diffusion increases by ~30% from 300 to 360 K in the simulation. An increase in the confining radius is also observed over the temperature range but are all in a similar range

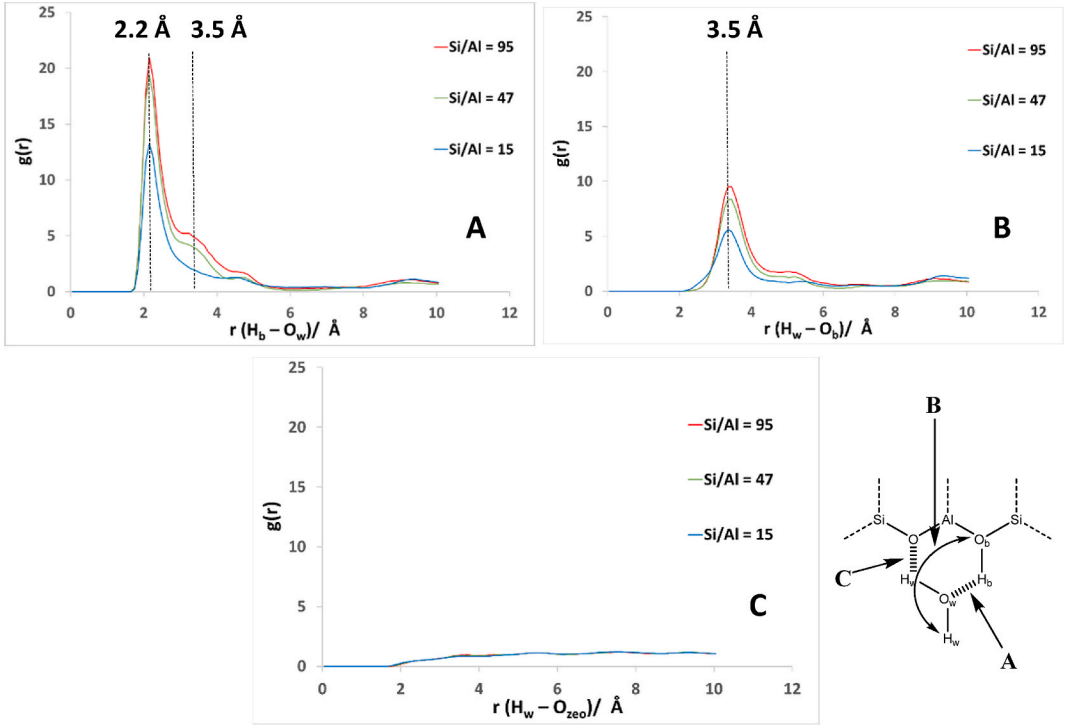

Fig. 12. RDFs illustrating various possible hydrogen bonds between water and the H-ZSM-5 framework where (a) shows the H_b (proton of the BAS) - O_w (oxygen of the water) distance (b) shows H_w (hydrogen of the water) - O_b (oxygen of the BAS) distance and (c) shows H_w - O_{zeo} (oxygen of the zeolite framework).

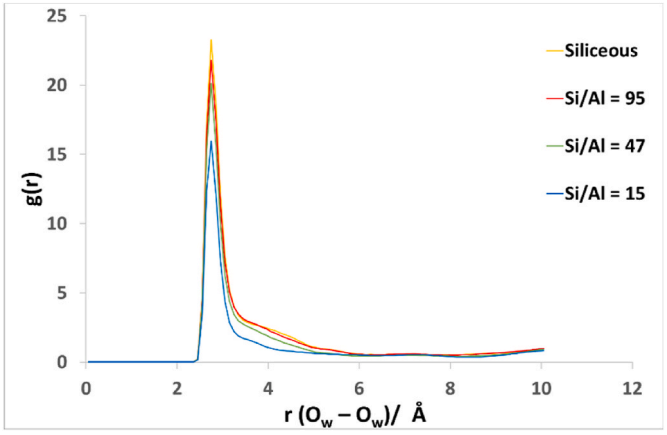

Fig. 13. RDFs illustrating water oxygen to water oxygen distances within the Si/Al = 15, 47 and 95 MFI type zeolite systems at 300 K.

to those determined from the QENS experiment. The sphere radius tends to be larger at the higher Si/Al ratios with the highest radii being around 6.2 Å, suggesting that the water has more freedom to move in the more siliceous systems. This may be because incorporation of BAS into the cages of the zeolite reduces the spherical volume available for the water to diffuse in [14].

The decay constants of the two exponential functions used to fit our MD calculated ISFs are equivalent to the widths of two separate Lorentzian functions used to fit the QENS spectra. One of these exponentials is outside of the dynamic range observable by the OSIRIS spectrometer representing a function with a HWHM as high as 1.4 meV – where OSIRIS measures energy transfers ±0.55 meV. A broadening this large would lead to its incorporation into the background function, and thus could not be observed on the timescales of our experiments. This represents a very fast localised motion and could be the isotropic rotation which has been shown to contribute to the model fitting of the MD calculated EISFs. The exponential decay with a lower decay constant (representing a lower energy motion within the instrumental time range) has been further analysed. This decay is the equivalent of the HWHM of the QENS line broadening, plotted as a function of Q^2 for the Si/Al = 15 H-ZSM-5 system in Fig. 15..

A deviation from linearity at higher Q values, indicative of jump diffusion, is observed and the Singwi-Sjölander (SS) jump diffusion model – described in SI section 1.2– gives the best fit across all systems as shown in experiment. Given the confinement suggested by the fitting of the EISF, the Q values that fall in a Q range representing a length above that commensurate with the radius of the confining sphere (~4 Å) are excluded from the fitting, although still included in the plot. These points at low Q, much like in experiment, deviate from the model due to confinement as the molecules show no translational motion of this length over the timescale sampled in our simulation.

Both the jump lengths and residence times can be extracted from these fits thus allowing the calculation of a diffusion coefficient. These parameters are listed in Table 5.

Although the calculated diffusion coefficients are very similar, the residence times are certainly larger on average in the simulation compared to those from experiment, particularly at higher temperatures (~18 ps across all systems from MD compared to ~7 ps from QENS). This is due to the fact that the diffusion coefficient is a factor of the jump distance squared and thus the change in residence time has a much smaller impact. The clear difference between the Si/Al = 15 & 40 and the Si/Al = 140 system are not reproduced by ISF analysis from the MD simulations. A comparison of the fitting parameters for both QENS and MD simulated QENS observables is shown in SI 2.3. This difference is clearer in the MSD analysis where a decrease in diffusivity is observed at the two lower Si/Al ratios. Evidently, probing different timescales has a significant effect on the observed behaviour and thus a combination of these two analyses must be considered when comparing such classical simulations to the QENS experiments.

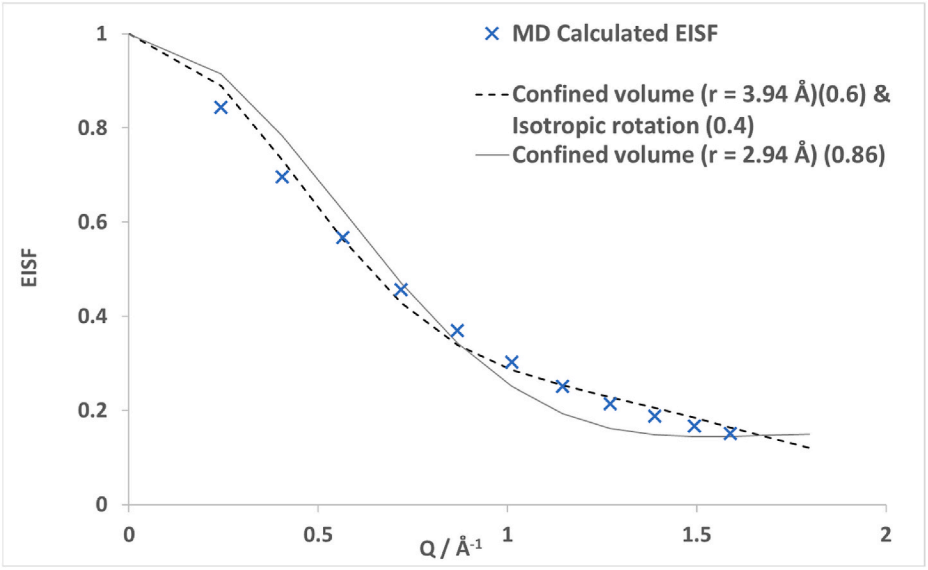

Fig. 14. MD calculated elastic incoherent structure factor, and models fitting this function, for water in the siliceous MFI framework at 300 K.

Table 4
Calculated confined volume radii and the contribution of the confined diffusion model to the EISF fits which was a linear combination of an isotropic rotation model and a model of confined diffusion.

	300 K		330 K		360 K	
Si/Al Ratio	**Confined Sphere Radius (Å)**	**Fraction of VD model**	**Confined Sphere Radius (Å)**	**Fraction of VD model**	**Confined Sphere Radius (Å)**	**Fraction of VD model**
15	3.8	0.59	4.1	0.71	4.9	0.78
47	3.5	0.57	4.0	0.69	4.8	0.78
95	3.5	0.57	4.4	0.70	5.2	0.79
∞	3.9	0.60	4.3	0.70	6.2	0.77

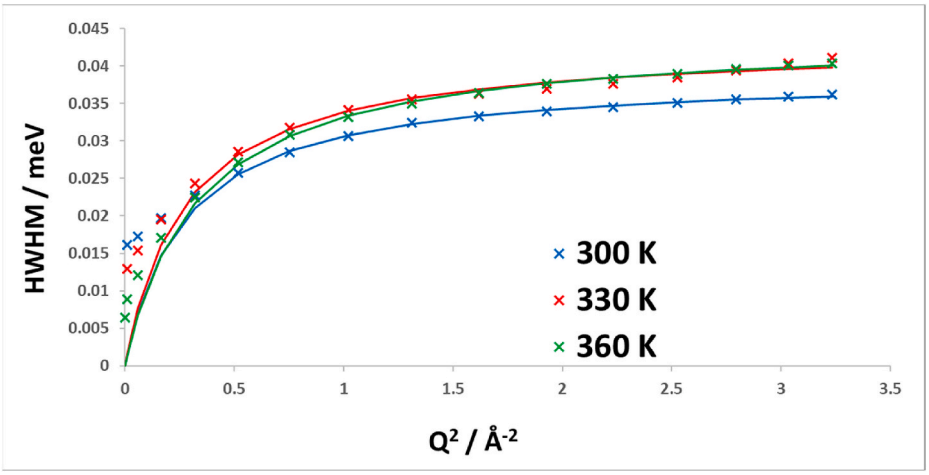

Fig. 15. Calculated decay constants of the exponential fit for the MD calculated ISFs, plotted as a function of Q, of water the Si/Al = 15 H-ZSM-5 framework at 300, 330 and 360 K.

5. Conclusions and outlook

Quasielastic neutron scattering (QENS) experiments, complemented by molecular dynamics (MD) simulations, have been used to probe the behaviour of water confined in H-ZSM-5 zeolites as a function of Si/Al ratio. QENS experiments were performed between 300 K and 360 K on H-ZSM-5 samples with Si/Al ratios of 15, 40 and 140 at water loadings of 2.8 wt%. MD simulations were run on the H-ZSM-5 systems with Si/Al ratios of 15, 47, 95 and a fully siliceous framework at water loadings of 2.8 wt% (9 MPUC) across the same temperature range.

The QENS experiments show confined water diffusion within the MFI pores at lower Si/Al ratios, with longer range, less confined diffusion in the more siliceous sample. Fitting of the EISF found that water diffusion confined to a sphere to be the best model to fit the experimental data, with spheres of radii ranging from 3.4 to 6.8 Å, with the larger radii in the more siliceous systems suggesting that the inclusion of BASs in the system reduce the volume available for diffusion, as seen in previous studies of methanol diffusion in the same framework [14]. An immobile

Table 5
Calculated jump lengths (to closest 0.25 Å), residence times (to closest 0.5 ps) and diffusion coefficients from the fits of Singwi-Sjölander jump diffusion model to the simulated QENS broadenings.

	300 K			330 K			360 K		
Si/Al Ratio	Jump distance (Å)	Residence time (ps)	Ds (10^{-9} m^2s^{-1})	Jump distance (Å)	Residence time (ps)	Ds (10^{-9} m^2s^{-1})	Jump distance (Å)	Residence time (ps)	Ds (10^{-9} m^2s^{-1})
15	2.00	17.0	2.18	2.00	15.0	2.38	1.75	15.0	2.03
47	2.00	18.0	2.25	1.25	15.0	1.04	2.25	18.5	2.45
95	1.25	15.5	1.12	1.75	16.5	1.73	2.50	18.5	3.46
∞	1.00	11.0	0.80	1.50	13.5	1.32	2.25	19.0	2.43

Diffusion coefficients calculated from these jump parameters ranged from ~0.8 to 3.5 × 10^{-9} m^2s^{-1} across all systems and temperatures and are similar to those measured by QENS (~0.9–4.8 × 10^{-9} m^2s^{-1}).

fraction was necessary to fit the experimental EISF, with ~30–80% of water molecules found to be mobile on the instrumental timescale, this fraction was observed to increase with both temperature and Si/Al ratio. Analysis of the quasielastic broadening indicated jump diffusion conforming to the Singwi-Sjölander model, with jump distances of ~1 Å and residence times ranging from ~9 to 4.5 ps. Shorter residence times were observed and thus higher D_s values were calculated (when this model was used) in the more siliceous systems. Diffusion coefficients ranging from ~1 to 5 × 10^{-9} m^2s^{-1} were calculated using the Volino-Dianoux model of diffusion confined to a sphere. The Si/Al = 15 and 40 systems did not yield diffusivities exceeding 2 × 10^{-9} m^2s^{-1}, however, the Si/Al = 140 system yielded diffusivities higher by a factor of 2–3 than those measured in the lower Si/Al systems, suggesting the lack of Brønsted sites in the system causes a significant increase in mobility.

The classical molecular dynamics simulations, when analysed on the nanoscale, yielded calculated self-diffusion coefficients ranging from 1.31 to 6.21 × 10^{-10} m^2s^{-1} in the siliceous system, and from 0.65 to 2.58 × 10^{-10} m^2s^{-1} in the Si/Al = 15 system between 300 K and 360 K. The lower diffusivities in the system with more Brønsted acid sites are attributed to strong coordination observed between the acid sites and the water molecules, where average residence times of 2–5 ps were measured and activation energies of diffusion of ~20 kJ mol^{-1} were calculated across all systems. QENS observables were reproduced from the MD trajectories such as the EISF and quasielastic broadenings. The MD calculated EISF gave the best fit to a combination of an isotropic rotation model – the contribution of which reduces with both temperature and Si/Al due to the lower density of BASs – the Volino-Dianoux model of diffusion confined to a sphere with radii ranging from 3.5 to 6.2 Å across all systems, consistent with that of experiment. However, the significant differences in diffusive behaviour between the low and high Si/Al ratios observed by QENS are not seen when our MD simulations are analysed on the timescale of ~100 ps (but are reproduced when the MD simulations are sampled over the nanosecond scale). Analysis of the quasielastic broadenings calculated from our MD simulations also showed jump-diffusion behaviour with diffusion coefficients ranging from ~0.8 to 3.5 × 10^{-9} m^2s^{-1} which is also in a similar range to that observed in the QENS experiments.

With respect to the studies discussed in the introduction, our study reveals some interesting points of comparison. Humplik et al. [15] observed a change in diffusivity of 2 orders of magnitude from a fully siliceous MFI sample to Si/Al = 100. This is significantly larger than the change observed in our study, which is less than one order of magnitude over a much larger Si/Al ratio range. This highlights the importance of probing multiple scales, as the referenced study was conducted using macro-scale infiltration experiments which may be influenced by more crystallite scale phenomena than QENS experiments. Bussai et al. [30] however, reported similar diffusion coefficients to those in the current work using PFG-NMR (~1.7 × 10^{-9} m^2s^{-1}) in silicalite. Ari et al. [16] reported diffusion coefficients around one order of magnitude lower than those reported here in the sodium containing form of ZSM-5 using molecular dynamics simulations. They also observed a decrease in diffusion coefficient by a factor of 5 between the fully siliceous and an Si/Al = 95 system, which is much larger than we report. This was likely caused by the much higher strength of interaction between water and sodium than that between water and a BAS. Such an observation illustrates the need for specific study of the effects of both Si/Al ratio and charge compensating species on adsorbate diffusion, as some very clear differences in trends appear due to the interplay between interaction strength, quantity, and location of such adsorption sites.

It was reported by Olson et al. [65] that "Heats of adsorption are shown to be a monotonic function of the number of water molecules adsorbed per H(Al) unit and independent of the framework aluminium content of the zeolite." – this shows that loading would likely play a significant role in the diffusivity of water as we have shown in our previous work [19], and that any in mobility with Si/Al ratio must be considered in this context. Joshi et al. [29] showed that the protonation of water clusters also had a loading dependency – we suspect that this would also contribute to diffusion properties as charged hydroxonium species may require hydration, similar to sodium, and the necessary clustering may reduce the average diffusivity. Our observations also provide experimental support for recent simulations suggesting that hydrated hydroxonium ions are formed within the channel intersections [59], where our confined restricted diffusion was observed.

When considering the implications of our findings for catalyst optimisation, where the H-ZSM-5 catalysed methanol to hydrocarbons process provides the most direct context for our systems, characterising and quantifying water mobility and the influence of BASs may bring us a step closer towards understanding factors governing the formation of the first C–C bond. The adsorption, desorption and diffusion properties of methanol and DME have been obtained in our previous studies [14]. However, in the equilibration reaction, water is a key species which could alter C–C bond formation depending on its competitive diffusion and adsorption properties, or dynamical effects on the reactive species present. Water may influence the adsorption and desorption of methanol and dimethyl ether or could preferentially occupy active sites and reduce reaction rates. Water which is more mobile, such as that observed in the ZSM-5 intersections, may be less likely to competitively adsorb in such a way, so designing a catalyst where the acidic sites are in the intersections may be favourable in this regard. Upon obtaining diffusion, adsorption and desorption properties, the Stefan-Maxwell and continuity equations may be applied to obtain concentration gradients across the pore length, indicative of reactant selectivity and catalyst efficiency during methanol-to-hydrocarbons catalysis. Quantitatively such values will be of great value to future multiscale kinetic models associated with catalytic processes [66].

A more general discussion on the behaviour of adsorbates in zeolites as a function of composition involves their potential as water decontamination technologies. Any separation process requires a significantly different diffusion coefficient between mixed components, and future avenues include in-depth studies of nanoscale diffusivity of pollutants, be it heavy metals [67] (though neutron scattering cross section may be a limiting factor) hydrogenous species [68] or more emerging pharmaceutical contaminants [69], where so far, the study of adsorption properties has taken precedence over understanding dynamical

properties such as diffusion. Our observation of the most mobile water being located in the channel intersections may be well be of direct consequence for the design of separation materials. Indeed, our relatively recent neutron spin echo/MD studies [70] observed that bulky branched molecules such as isobutane reside in small sections of sinusoidal channel which may have implications for removal of bulky spherical pollutants, and it may be preferable to design any MFI based decontaminant material with the adsorption site in the intersections, where the difference in diffusivity between contaminant and water will be most significant (due to the increased mobility of water in this location) and competitive adsorption will therefore be minimised.

Indeed, while our study has uncovered the complexity of water behaviour in such a commercially relevant catalyst, future studies probing these time and length scales and their correlation with macroscale observations, whether it be catalytic activities/selectivities or separation/adsorption properties will be important for the screening of potential materials and optimising their structure and composition for such technologies.

CRediT authorship contribution statement

A.J. Porter: Writing – review & editing, Writing – original draft, Validation, Software, Investigation, Formal analysis. **S.L. McHugh:** Investigation. **T. Omojola:** Writing – review & editing, Funding acquisition, Conceptualization. **I.P. Silverwood:** Writing – review & editing, Resources, Methodology, Investigation. **A.J. O'Malley:** Writing – review & editing, Writing – original draft, Supervision, Investigation, Funding acquisition, Conceptualization.

Declaration of competing interest

The authors declare that they have no known competing financial interests or personal relationships that could have appeared to influence the work reported in this paper.

Data availability

Data DOI is shared in acknowledgements

Acknowledgements

This work was supported by the UK Engineering and Physical Sciences Research Council (EPSRC), grant nos. EP/R513155/1 and EP/L016354/1 at the University of Bath. The work has made use of the Balena High Performance Computing (HPC) Service at the University of Bath. AJOM acknowledges Roger and Sue Whorrod for the funding of a Whorrod Fellowship. TO acknowledges Andre van Veen for fruitful scientific discussions. The ISIS Neutron and Muon Source at the STFC Rutherford Appleton Laboratory are thanked for access to neutron beam facilities; the data from our experiment RB 1920014 can be found at DOI: 10.5286/ISIS.E.RB1920014-1. We would also like to thank Dr Rémi Castaing for the running and maintenance of the TGA analyser as well as the whole of MC^2 at the University of Bath.

Appendix A. Supplementary data

Supplementary data to this article can be found online at https://doi.org/10.1016/j.micromeso.2022.112391.

References

[1] J. Kärger, S. Vasenkov, S.M. Auerbach, Handbook of Zeolite Science and Technology, CRC Press, 2003, pp. 458–560.
[2] K. Margeta, N.Z. Logar, M. Šiljeg, A. Farkaš, Water Treat. 5 (2013) 81–112.
[3] J. Cejka, H. van Bekkum, A. Corma, F. Schueth, Introduction to Zeolite Molecular Sieves, 3 edn., Elsevier Science, 2007.
[4] K. Chen, J. Damron, C. Pearson, D. Resasco, L. Zhang, J.L. White, ACS Catal. 4 (2014) 3039–3044.
[5] R. Krishna, J.M. van Baten, Langmuir 26 (2010) 10854–10867.
[6] I. Yarulina, A.D. Chowdhury, F. Meirer, B.M. Weckhuysen, J. Gascon, Nature Catalysis 1 (2018) 398–411.
[7] M.E. Potter, S. Chapman, A.J. O'Malley, A. Levy, M. Carravetta, T.M. Mezza, S. F. Parker, R. Raja, ChemCatChem 9 (2017) 1897–1900.
[8] E.G. Derouane, J.C. Védrine, R.R. Pinto, P.M. Borges, L. Costa, M.A.N.D.A. Lemos, F. Lemos, F.R. Ribeiro, Catal. Rev. 55 (2013) 454–515.
[9] A. Palčić, V. Valtchev, Appl. Catal. Gen. 606 (2020), 117795.
[10] C.-L.M. Woodward, A.J. Porter, K.S. Morton, A.J. O'Malley, Catal. Commun. 164 (2022), 106415.
[11] C.H. Botchway, R. Tia, E. Adei, A.J. O'Malley, N.Y. Dzade, C. Hernandez-Tamargo, N.H. de Leeuw, Catalysts 10 (2020) 1342.
[12] L. Parker, D. Bibby, G. Burns, Zeolites 11 (1991) 293–297.
[13] M.W. Anderson, J. Klinowski, P.J. Barrie, J. Phys. Chem. 95 (1991) 235–239.
[14] T. Omojola, I.P. Silverwood, A.J. O'Malley, Catal. Sci. Technol. 10 (2020) 4305–4320.
[15] T. Humplik, R. Raj, S.C. Maroo, T. Laoui, E.N. Wang, Langmuir 30 (2014) 6446–6453.
[16] M.U. Ari, M.G. Ahunbay, M. Yurtsever, A. Erdem-Senatalar, J. Phys. Chem. B 113 (2009) 8073.
[17] H. Paoli, A. Méthivier, H. Jobic, C. Krause, H. Pfeifer, F. Stallmach, J. Kärger, Microporous Mesoporous Mater. 55 (2002) 147–158.
[18] A. Özgür Yazaydın, R.W. Thompson, Microporous Mesoporous Mater. 123 (2009) 169–176.
[19] A.J. Porter, A.J. O'Malley, J. Phys. Chem. C 125 (2021) 11567–11579.
[20] C. Parravano, J.D. Baldeschwieler, M. Boudart, Science 155 (1967) 1535–1536.
[21] W. Wang, M. Seiler, M. Hunger, J. Phys. Chem. B 105 (2001) 12553–12558.
[22] S. Svelle, S. Kolboe, O. Swang, U. Olsbye, J. Phys. Chem. B 109 (2005) 12874–12878.
[23] T. Omojola, N. Cherkasov, A.I. McNab, D.B. Lukyanov, J.A. Anderson, E.V. Rebrov, A.C. van Veen, Catal. Lett. 148 (2018) 474–488.
[24] J. Valecillos, G. Elordi, A.T. Aguayo, P. Castaño, Catal. Sci. Technol. 11 (2021) 1269–1281.
[25] S. Eckstein, P.H. Hintermeier, R. Zhao, E. Baráth, H. Shi, Y. Liu, J.A. Lercher, Angew. Chem. Int. Ed. 58 (2019) 3450–3455.
[26] N. Pfriem, P.H. Hintermeier, S. Eckstein, S. Kim, Q. Liu, H. Shi, L. Milakovic, Y. Liu, G.L. Haller, E. Baráth, Science 372 (2021) 952–957.
[27] D. Olson, W. Haag, W. Borghard, Microporous Mesoporous Mater. 35 (2000) 435–446.
[28] D. Mei, J.A. Lercher, AIChE J. 63 (2017) 172–184.
[29] K.L. Joshi, G. Psofogiannakis, A.C.T. van Duin, S. Raman, Phys. Chem. Chem. Phys. 16 (2014) 18433–18441.
[30] C. Bussai, S. Vasenkov, H. Liu, W. Böhlmann, S. Fritzsche, S. Hannongbua, R. Haberlandt, J. Kärger, Appl. Catal. Gen. 232 (2002) 59–66.
[31] A.J. O'Malley, C.R.A. Catlow, Experimental methods in the physical Sciences, in: F. Fernandez-Alonso, D.L. Price (Eds.), Academic Press, vol. 49, 2017, pp. 349–401.
[32] J. Armstrong, A.J. O'Malley, M.R. Ryder, K.T. Butler, J. Phys. Commun. 4 (2020), 072001.
[33] H. Jobic, D.N. Theodorou, Microporous Mesoporous Mater. 102 (2007) 21–50.
[34] A.J. O'Malley, S.F. Parker, C.R.A. Catlow, Chem. Commun. 53 (2017) 12164–12176.
[35] M. Trzpit, M. Soulard, J. Patarin, N. Desbiens, F. Cailliez, A. Boutin, I. Demachy, A. H. Fuchs, Langmuir 23 (2007) 10131–10139.
[36] M.T. Telling, K.H. Andersen, Phys. Chem. Chem. Phys. 7 (2005) 1255–1261.
[37] R.T. Azuah, L.R. Kneller, Y. Qiu, P.L. Tregenna-Piggott, C.M. Brown, J.R. Copley, R. M. Dimeo, J. Res. National Inst. Standard Technol. 114 (2009) 341.
[38] O. Arnold, J.-C. Bilheux, J. Borreguero, A. Buts, S.I. Campbell, L. Chapon, M. Doucet, N. Draper, R.F. Leal, M. Gigg, Nucl. Instrum. Methods Phys. Res. Sect. A Accel. Spectrom. Detect. Assoc. Equip. 764 (2014) 156–166.
[39] W.M. Meier, D.H. Olson, C. Baerlocher, Zeolites 17 (1996) 1–229.
[40] A.R. Ruiz-Salvador, R. Grau-Crespo, A.E. Gray, D.W. Lewis, J. Solid State Chem. 198 (2013) 330–336.
[41] R. Grau-Crespo, A.G. Peralta, A.R. Ruiz-Salvador, A. Gómez, R. López-Cordero, Phys. Chem. Chem. Phys. 2 (2000) 5716–5722.
[42] E. Dempsey, J. Catal. 49 (1977) 115–119.
[43] T.G.A. Youngs, J. Comput. Chem. 31 (2010) 639–648.
[44] K.-P. Schröder, J. Sauer, M. Leslie, C. Richard, A. Catlow, J.M. Thomas, Chem. Phys. Lett. 188 (1992) 320–325.
[45] M.J. Sanders, M. Leslie, C.R.A. Catlow, J. Chem. Soc., Chem. Commun. (1984) 1271–1273.
[46] C.R.A. Catlow, R. James, W.C. Mackrodt, R.F. Stewart, Phys. Rev. B 25 (1982) 1006–1026.
[47] N.A. Ramsahye, R.G. Bell, J. Phys. Chem. B 109 (2005) 4738–4747.
[48] Farragher Kramer, B. van Beest, R. van Santen, Phys. Rev. B 43 (1991) 5068.
[49] I.T. Todorov, W. Smith, K. Trachenko, M.T. Dove, J. Mater. Chem. 16 (2006) 1911–1918.
[50] H.J.C. Berendsen, J.P.M. Postma, W.F. van Gunsteren, A. Dinola, J.R. Haak, J. Chem. Phys. 81 (1984) 3684–3690.
[51] U.W. Schmitt, G.A. Voth, J. Chem. Phys. 111 (1999) 9361–9381.
[52] Z. Du, N.H. de Leeuw, Surf. Sci. 554 (2004) 193–210.
[53] D.W. Lewis, A.R. Ruiz-Salvador, N. Almora-Barrios, A. Gómez, M. Mistry, Mol. Simulat. 28 (2002) 649–661.
[54] W. Humphrey, A. Dalke, K. Schulten, J. Mol. Graph. 14 (1996) 33–38.

[55] A.J. O'Malley, M. Sarwar, J. Armstrong, C.R.A. Catlow, I. Silverwood, A. York, I. Hitchcock, Phys. Chem. Chem. Phys. 20 (2018) 11976–11986.
[56] K. Singwi, A. Sjölander, Phys. Rev. 119 (1960) 863.
[57] M. Holz, S.R. Heil, A. Sacco, Phys. Chem. Chem. Phys. 2 (2000) 4740–4742.
[58] M. Wang, N.R. Jaegers, M.-S. Lee, C. Wan, J.Z. Hu, H. Shi, D. Mei, S.D. Burton, D. M. Camaioni, O.Y. Gutiérrez, V.-A. Glezakou, R. Rousseau, Y. Wang, J.A. Lercher, J. Am. Chem. Soc. 141 (2019) 3444–3455.
[59] E. Grifoni, G. Piccini, J.A. Lercher, V.-A. Glezakou, R. Rousseau, M. Parrinello, Nat. Commun. 12 (2021) 2630.
[60] Y. Liu, A. Vjunov, H. Shi, S. Eckstein, D.M. Camaioni, D. Mei, E. Baráth, J. A. Lercher, Nat. Commun. 8 (2017) 1–8.
[61] B. Hunger, M. Heuchel, S. Matysik, K. Beck, W. Einicke, Thermochim. Acta 269 (1995) 599–611.
[62] A. Ison, R.J. Gorte, J. Catal. 89 (1984) 150–158.
[63] H. Jobic, A. Tuel, M. Krossner, J. Phys. Chem. 100 (50) (1996) 19545–19550.
[64] M. Krossner, J. Phys. Chem. 100 (15) (1996) 6199–6211.
[65] D.H. Olson, W.O. Haag, W.S. Borghard, Microporous Mesoporous Mater. 35–36 (2000) 435–446.
[66] C. Zhang, K.L.A. Ng, L. Yan, X. Feng, B. Jiang, Z. Liao, J. Wang, Y. Yang, Ind. Eng. Chem. Res. 61 (2022) 2055–2067.
[67] C. Hernandez-Tamargo, B. Kwakye-Awuah, A.J. O'Malley, N.H. de Leeuw, Microporous Mesoporous Mater. 315 (2021), 110903.
[68] J.B. Awuah, N.Y. Dzade, R. Tia, E. Adei, B. Kwakye-Awuah, C. Richard A. Catlow, N.H. de Leeuw, Phys. Chem. Chem. Phys. 18 (2016) 11297–11305.
[69] M. Fischer, Mater. Adv. 1 (2020) 86–98.
[70] A.J. O'Malley, C.R.A. Catlow, M. Monkenbusch, H. Jobic, J. Phys. Chem. C 119 (2015) 26999–27006.